Astronomy & Astrophysics

INTEGRAL observations of the Crab pulsar[*]

T. Mineo[1], C. Ferrigno[1], L. Foschini[2], A. Segreto[1], G. Cusumano[1], G. Malaguti[2], G. Di Cocco[2], and C. Labanti[2]

[1] INAF IASF-Pa, via U. La Malfa 153, 90146 Palermo, Italy
  e-mail: teresa.mineo@ifc.inaf.it
[2] INAF IASF-Bo, via P. Gobetti 101, 40129 Bologna, Italy

ABSTRACT

Aims. The paper presents the timing and spectral analysis of several observations of the Crab pulsar performed with INTEGRAL in the energy range 3–500 keV.
Methods. All these observations, when summed together provide a high statistics data set which can be used for accurate phase resolved spectroscopy. A detailed study of the pulsed emission at different phase intervals is performed.
Results. The spectral distribution changes with phase showing a characteristic reverse S shape of the photon index. Moreover the spectrum softens with energy, in each phase interval, and this behavior is adequately modeled over the whole energy range 3–500 keV with a single curved law with a slope variable with $\mathrm{Log}(E)$, confirming the BeppoSAX results on the curvature of the pulsed emission. The bending parameter of the log-parabolic model is compatible with a single value of 0.14 ± 0.02 over all phase intervals.
Conclusions. Results are discussed within the three-dimensional outer gap model.

Key words. stars: neutron – pulsars: general – pulsars: individual: PSR B0531+21 – X-rays: stars

1. Introduction

The Crab pulsar (PSR B0531+21) can be observed in almost every energy band of the electromagnetic spectrum. Its pulse profile is characterized by a double peak structure with a phase separation of 0.4 that is almost aligned in absolute phase over all wavelengths (Rots et al. 2004; Kuiper et al. 2003; Tennant et al. 2001).

In the X-ray range, the relative intensity, height and width of the two peaks vary with energy: the first peak (P1), dominant at low X-ray energies, becomes smaller than the second one (P2). Moreover, an enhancement with energy of the bridge between these peaks, usually called Interpeak (Ip), is also well evident (Mineo et al. 1997, see also Fig. 1). At energy above 1 MeV, the morphology changes abruptly: the first pulse becomes again dominant over the second one and the bridge emission loses significance; the pulse profile above 30 MeV is similar to the one observed at optical wavelengths (Kuiper et al. 2001).

A first detailed study of the phase-resolved X-ray spectra has been performed by Pravdo et al. (1997), in the 5–200 keV energy interval, based on RXTE (PCA and HEXTE) data. Their main result was a variation of the photon index as function of the pulse phase with a reverse S shape: the spectrum softens starting from the leading edge of the first peak where it

reaches the maximum value, it hardens in the interpeak and softens again in the second peak. The S shape spectral variation with phase has been reported by Massaro et al. (2000) from BeppoSAX data and by Weisskopf et al. (2004) from Chandra data, even if with lower statistical significance, confirming the symmetric evolution of the spectral index around the first peak. However, the softening of the P1 core respect to the leading edge has been recently questioned by Vivekanand (2002) in a new analysis of RXTE data but performed over the smaller energy range of 5–60 keV.

Significant X-ray emission from the pulsar in the off-pulse interval (phase 0.5–0.9) was discovered by Tennant et al. (2001) with Chandra observations, however, the spectral index measured in this phase interval suffers of large statistical uncertainty (Weisskopf et al. 2004).

BeppoSAX observations of the Crab pulsar showed that the photon indices of the pulsed emission significantly increase with energy maintaining the same S shape behavior over the 0.1–300 keV energy range (Massaro & Cusumano 2003; Zhang & Cheng 2002). The spectral index variation has been modeled using a single curved power law with a slope variable with $\mathrm{Log}(E)$ (Massaro et al. 2000). Moreover, applying this model to three wide phase intervals, the first peak, the Interpeak and the second peak, a single value of ~0.15 for the curvature parameter has been measured in the three intervals (Massaro et al. 2001).

---

[*] Appendix A is only available in electronic form at
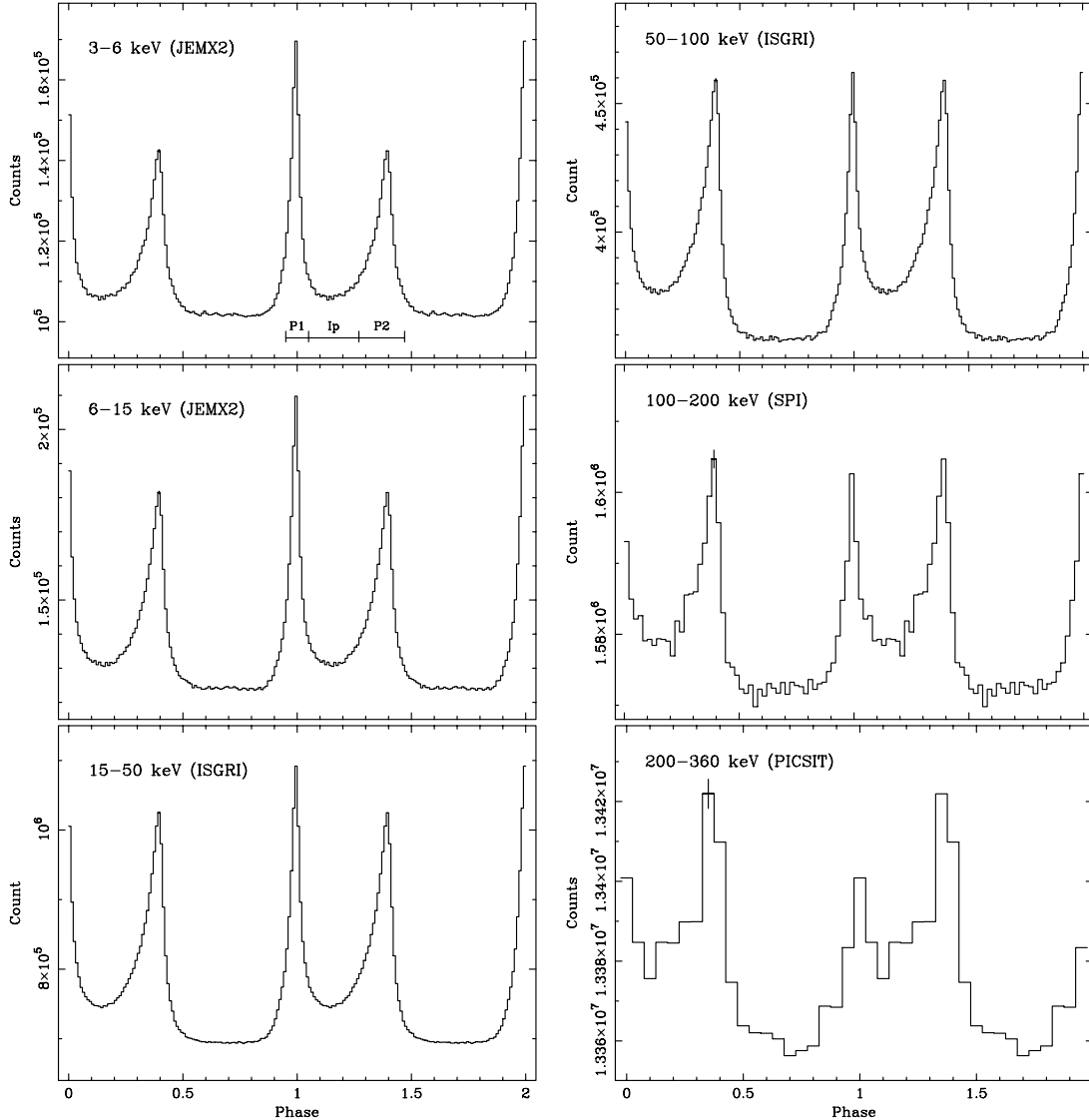http://www.edpsciences.org

Fig. 1. Crab phase histograms in six energy bands in absolute phase (the main radio pulse at phase 0.0). The light curves have different phase resolution according to the statistics available and to the time resolution of the instrument. P1, P2 and Ip phase intervals according to the definition given in Mineo et al. (1997) are indicated in the top left panel.

Kuiper et al. (2001) presented a coherent high-energy picture of the Crab pulsar from 0.1 keV up to 10 GeV by using the high energy γ-ray data from the CGRO satellite together with data obtained at X-ray energies from several observatories. The authors model the 0.1 keV–10 GeV pulsed emission in 7 narrow phase slices with a composite model: a power law present in the phase intervals of the two main pulses, a curved spectral component required in the same phase intervals and second broader curved spectral component representing mainly the bridge emission.

X-ray observations of Crab pulsar performed with a balloon born experiment report the detection of an emission line at 440 keV with a flux of $(0.86\pm0.33)\times10^{-4}$ ph cm^{-2} s^{-1} (Massaro et al. 1991). Ulmer et al. (1994), using OSSE data, did not detected this line but derived a 3σ upper limit compatible with its presence.

Results on the INTEGRAL observations of the Crab pulsar have already been presented by Kuiper et al. (2003), that

studied the instrument absolute timing accuracy and by Brandt et al. (2003) who reports results on the 3–37 keV energy range with the X-ray monitor JEM-X.

In this paper, we present the timing and spectral analysis of several observations of the Crab pulsar performed with SPI, JEM-X, IBIS/ISGRI and IBIS/PICsIT on board INTEGRAL. We investigate the presence of the 440 keV line and thanks to the wide energy range covered by INTEGRAL instruments and to the good statistics achieved by the summed data sets, we are able to perform a detailed phase resolved spectroscopy on the Crab pulsed emission over the wide energy range 3–500 keV.

2. Observation and data reduction

The International Gamma-Ray Astrophysics Laboratory (INTEGRAL; Winkler et al. 2003) observed the Crab nebula and pulsar for calibration purposes several times from February 2003 (rev. 39) to August 2003 (rev. 103).

Table 1. Observation log for the data used in this analysis.

Revolution	Start-Stop time	Exposure (ks)			
	(MJD)	JEM-X	ISGRI	PICsIT	SPI
39	52677.2–52679.8	149.3	142.3	–	–
40	52680.2–52681.6	122.6	56.0	106.5	–
41	52683.2–52685.8	–	–	204.0	–
42	52686.4–52688.2	75.4	61.6	–	138.5
43	52689.6–52691.7	–	30.7	–	154.9
44	52692.2–52694.4	–	9.8	–	146.9
45	52695.2–52696.7	–	2.1	–	27.4
102	52866.3–52868.1	–	37.9	–	78.0
103	52868.6–52868.8		21.6	–	–
Total		347.3	362.0	310.5	545.7

The INTEGRAL payload is composed of three high energy instruments. JEM-X (Lund et al. 2003) consists of two identical coded-aperture mask telescopes with a geometrical area of 500 cm^2 and an angular resolution of 3 arcmin across an effective field of view of about 10°. The detector at the focal plane, a Microstrip Gas Chamber, operates in the energy range 3–35 keV with an energy resolution of ~17% at 6 keV. SPI (Vedrenne et al. 2003) is a high spectral resolution gamma-ray telescope that consists of an array of 19 closely packed germanium detectors surrounded by an active anticoincidence shield of BGO. The imaging capabilities of the instrument are obtained with a tungsten coded aperture mask adopting a particular observing strategy (dithering). The fully coded field-of-view is 16°, and the angular resolution is 2.5°. The energy range extends from 20 keV to 8 MeV with a typical energy resolution of 2.5 keV at 1.3 MeV. IBIS (Ubertini et al. 2003) is a coded aperture telescope composed by two detection layers: ISGRI (Lebrun et al. 2003) and PICsIT (Di Cocco et al. 2003). ISGRI is a large CdTe gamma-ray camera operating in the range 15 keV–1 MeV, with a geometrical area of 2621 cm^2 and an energy resolution of ~8% at 60 keV. PICsIT is composed by 64×64 Caesium-Iodide (CsI) scintillation pixels working in the energy intervals 175 keV–10 MeV.

The limited telemetry budged of INTEGRAL degrades the event timing information on board. Taking into account all possible uncertainties affecting the time accuracy (the On Board Time (OBT) accuracy, the orbit prediction etc.), Kuiper et al. (2003) estimated that the resulting time resolution is 90 μs for IBIS, 130 μs for SPI and 150 μs for JEM-X, about 30–40% worse than the nominal time resolution of each single instrument; moreover the INTEGRAL absolute timing accuracy, as estimated by Kuiper et al. (2003) from Crab data, is about 40 μs. The IBIS/PICsIT detector cannot be routinely configured in photon-by-photon mode due to the high telemetry budget requested for this operational mode. For timing studies then, observers can select the spectral-timing mode in which the whole detector counts are accumulated on board in up to eight energy bands (default 4) and with an integration time in the range 0.97–500 ms (default 3.9 ms).

The analysis performed in this paper uses on axis JEM-X observations and SPI data relative to pointings less than 6°.

IBIS observations have a maximum off-axis angle of 1°. They are relative to different configuration of the instrument: in particular, data are accumulated on board with different rise-time selections. We then verified that spectra relative to different science windows have negligible differences in the energy range considered for the spectral analysis. IBIS/PICsIT observation intervals with time resolution of 1 ms have been considered and to improve the statistics of the light curve, data from rev. 0041 with an off-axis of 9.6° were also included.

Table 1 summarizes the log of the observations used in this analysis together with the relative time exposures.

To obtain spectra and light curves of the sources present in the field, INTEGRAL official software (OSA[1]), whose algorithms are described in Goldwurm et al. (2003) and Gros et al. (2003) for IBIS, Skinner & Connell (2003), and Strong (2003) for SPI, and Westergaard et al. (2003) for JEM-X, repeats a shadowgram deconvolution process several times, by selecting events in the energy and time intervals of interest. However, when the source positions have already been determined (because a priori known or predetermined by a shadowgram deconvolution), it is alternatively possible, to select only the detector pixels fully illuminated by the source. This method simplifies the accumulation of phase resolved spectra. The amount of illumination from a given source, normalized to the maximum illumination value is called Photon Illumination Fraction (PIF) and is generated by the standard software for JEM-X and IBIS/ISGRI. For these instruments, we run the standard pipeline (OSA vers. 4.2) up to the "DEAD" level that includes the conversion from detector energy channels (PHA) to energy channels corrected for instrumental effects (PI), the selection for the Good Time Intervals (GTI) and the correction for the instrument dead time and we selected events with PIF = 1. However, IBIS/ISGRI conversion PHA-to-PI has been performed through our own calibration file generated by one of the authors (A.S.). This file is based on on-ground and in-flight calibration data and represents an improvement respect to the standard one (see Appendix A).

---

[1] Available at http://isdc.unige.ch/index.cgi?Soft+download

No PIF selection is possible for SPI; we then extracted the list files relative to the whole field of view running the standard pipeline (OSA vers. 4.2) up to the "COR" level that produces corrected events selected for the GTI.

The response matrices used in the analysis of JEM-X and SPI data are provided by the standard software. The ISGRI response matrix has been generated with our own software to take into account the new PHA-to-PI calibration file (see Appendix A).

No response matrix is available for spectral timing data with IBIS/PICsIT; the presently available matrices are in fact suitable only for spectral imaging data. Data from this detector have not been included in the spectral analysis.

JEM-X spectral analysis was performed in the energy range 3–20 keV, IBIS/ISGRI and SPI spectra were fitted in the range 20–500 keV and 40–200 keV, respectively.

Errors quoted in the paper are relative to 1σ confidence level for one interesting parameter.

3. Timing analysis

Arrival times were converted to the Solar System Barycentre with the DE200 ephemeris. The values of P and $\dot{P}$ in GRO format for each observation (our data set spans several months) were derived from Jodrell Bank Crab Pulsar Monthly Ephemeris (http://www.jb.man.ac.uk/) using contemporary radio ephemeris.

Phase histograms of the Crab pulsar were evaluated for each instrument and each observation using the period folding technique and adding the various offsets quoted in Walter et al. (2003) to correct the time relation derived by the INTEGRAL Science Data Center. The resulting phase histograms in six energy bands from 3 keV to 360 keV are shown in Fig. 1 in absolute phase with a phase resolution ranging from 0.01 (0.33 ms) to 0.03 (1.1 ms) according to the available statistics and to the instrument time resolution.

The well-known double peaked structure is prominent in all the profiles with a high statistical significance and the known evolution of the Crab pulse profile with energy can be observed: the relative intensity of the first pulse respect to the second increases with energies together with the level of the bridge emission.

4. Spectral analysis

Crab pulsar phase histograms with 100 phase bins for JEM-X1, JEM-X2 and IBIS/ISGRI and 50 phase bins for SPI were generated for each energy channel of each instrument and organized in an energy-phase matrix. A detailed phase resolved spectral analysis in the range (−0.1, +0.46) was performed by selecting spectra in phase intervals 0.01 wide in the two main peaks and 0.02 in the interpeak for JEM-X1, JEM-X2 and IBIS/ISGRI; phase intervals of double size (0.02 at the two peaks and 0.04 in the interpeak) were considered for SPI data. The nebular emission and the instrumental background for each phase resolved spectra were subtracted evaluating them from the off-pulse level in the pase interval (+0.60, +0.80) and

considering that the contribution of the pulsed emission in this phase interval is negligible (Weisskopf et al. 2004).

Energy channels are uniformly rebinned in agreement with the response matrices and in order to have a minimum bin content of 20 counts.

Spectra of each instrument were first modeled with a single power law; low energy absorption has been included in the JEM-X fits, fixing the absorbing column to the values derived by Weisskopf et al. (2004). Spectra from the two JEM-X units were fitted simultaneously introducing as free parameter a factor to take care of the instrumental systematics. The best fit values of this intercalibration factor are in the range 0.8–1.06 with an average of 0.98.

JEM-X reduced χ^2 are generally acceptable: they span the range 0.8 1.2 (d.o.f. 266) with only four values out of 42 above this range (between 1.29 and 1.33).

IBIS/ISGRI fits gave values of reduced χ^2 between 0.8 and 1.8 (122 d.o.f.) with 16 values greater than 1.26 over 42 and only one above 1.5. These higher values of reduced χ^2 can be considered acceptable because they are due to local residuals at low energies as expected from the level of accuracy of the systematics in OSA 4.2 software[2]. The SPI values of the reduced χ^2 lie in the expected range 0.7–1.4 (41 d.o.f.) with only two values at 1.6. The best fit spectral indices are shown in Fig. 2 vs. phase together with the light curves for the three instruments. As example in Fig. 3 (top panels) the JEM-X, IBIS/ISGRI and SPI spectra relative to the the first peak are shown together with the residuals respect to the simple power-law model (bottom panels).

The same phase dependence is clearly apparent in each plot in Fig. 2: the first peak has the softest spectrum, whereas the hardest emission is produced in the interpeak. The statistical significance of the softening of the spectral index has been evaluated fitting the photon index in the leading edge of the first peak with a constant and with a line. Applying the F-test to the derived χ^2, a significance of 99.6% in the JEM-X2 energy range and 99.7% in the IBIS/ISGRI 20–500 keV can be inferred confirming the results obtained by Pravdo et al. (1997) and Massaro et al. (2000).

The presence of a line at 440 keV in the ISGRI spectrum relative to the phase interval (0.27–0.47) has also been investigated. We find a 3σ upper limit of 1.4×10^{-3} ph cm^{-2} s^{-1} consistent with the presence of the line detected by Massaro et al. (1991).

Comparing JEM-X, SPI and IBIS/ISGRI results, we note that spectral indices are clearly increasing with energy over all the phase intervals, in agreement with BeppoSAX results (Massaro et al. 2000). It is already known that the spectral energy distribution of the Crab pulsed emission is continuously steepening from the optical frequencies to γ-rays. In the X-ray range, Massaro et al. (2000) showed that a suitable model is the curved power law with a continuously steepening described by the following formula:

$$F(E) = K \, E^{-(a+b\,\mathrm{Log}(E))} \tag{1}$$

---

[2] See the report osa_sci_val_isgri-1.0.pdf available at http://isdc.unige.ch/Soft/download/osa/osa_doc/prod
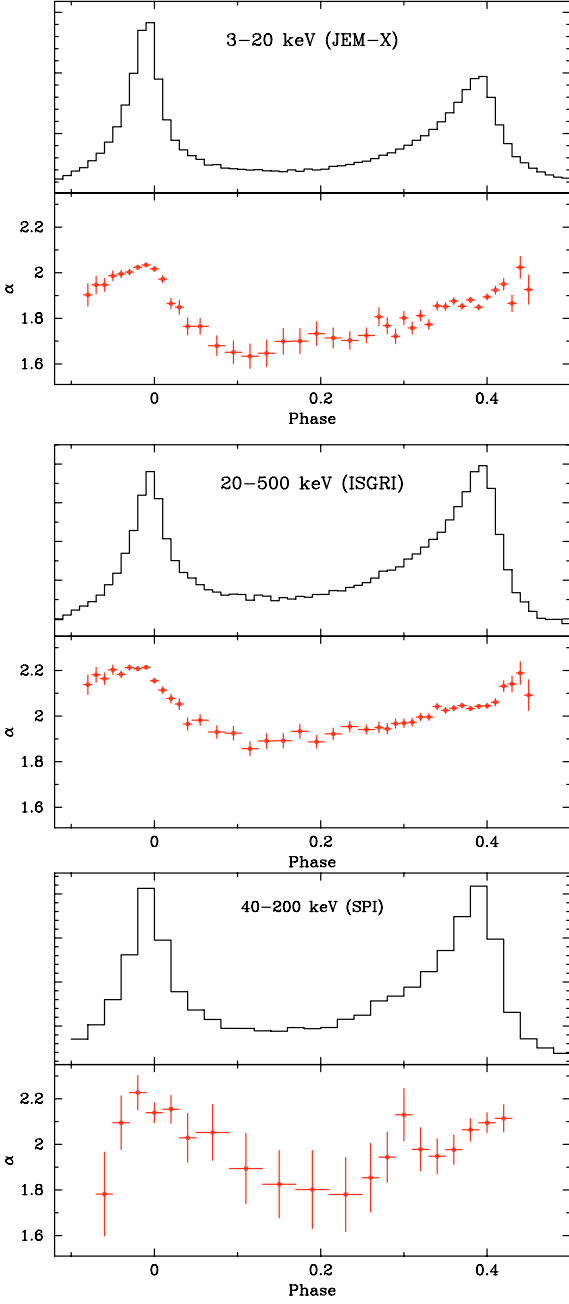
Fig. 2. Spectral index vs. phase measured by JEM-X in the energy range 3–20 keV (*top panel*), IBIS/ISGRI in the energy range 20–500 keV (*middle panel*) and SPI in the energy range 40–200 keV (*bottom panel*).

Fig. 3. JEM-X, IBIS/ISGRI and SPI spectrum of the phase interval 0.99–1.00 fitted with a single power law.

where a corresponds to the photon index at 1 keV and b measures the curvature of the spectral distribution.

We fitted at first JEM-X2 and ISGRI spectra simultaneously with a single power law introducing a normalization factor in the model to take into account the intercalibration systematics between the two instruments. In this wide band fits we considered only JEM-X2 units that shows a better calibration compared to the BeppoSAX-MECS. We find, in fact that the discrepancies in the photon indices measured by the two instruments, in the common energy range 2–10 keV, in the same phase intervals is lower than 5%. SPI has not been included
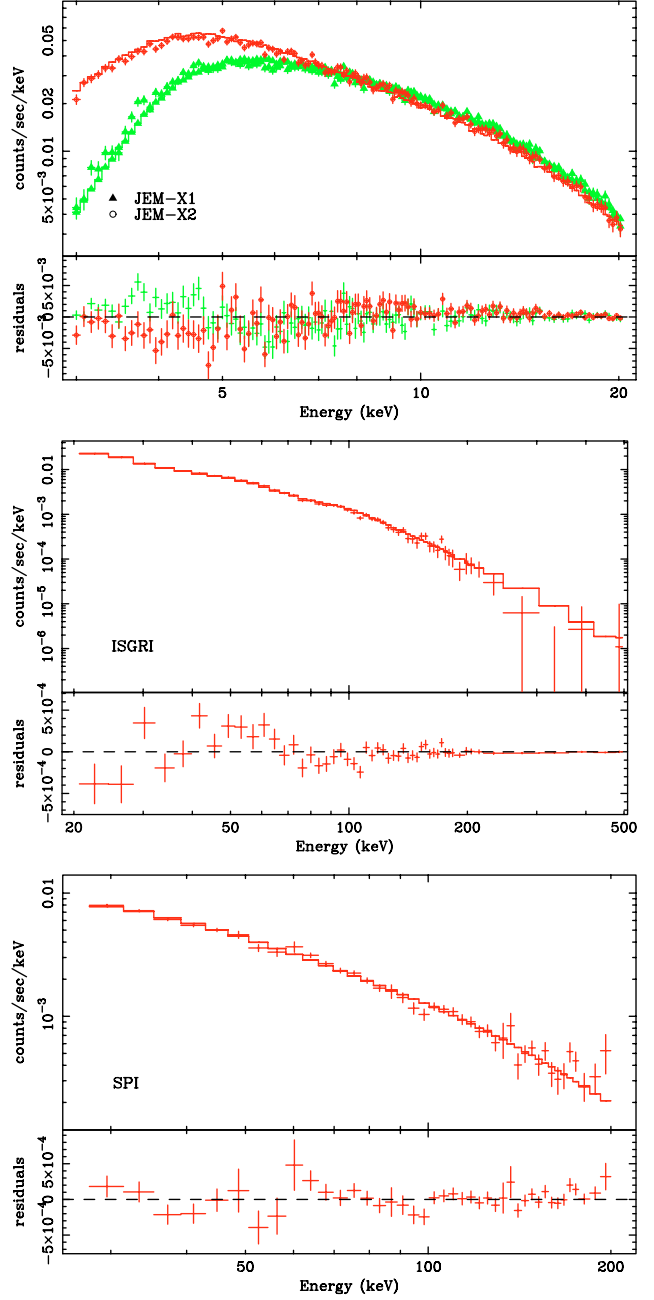
because of the lower statistics. The resulted reduced χ^2 have values generally unacceptable for the expected distribution with 256 degree of freedom. The distribution of the reduced χ^2 is shown in the top panel of Fig. 4: values >1.3 are relative to the spectra in the two main peaks. Following Massaro et al. (2000) approach, we fitted then JEM-X2 and ISGRI spectra simultaneously with the curved model of Eq. (1). All fits gave acceptable χ^2, as shown in the bottom panel of Fig. 4 and the best fit values of intercalibration factors are compatible with the constant 0.92 ± 0.01 over all phase intervals. The best fit values of the two parameters vs. phase are shown in Fig. 5. The bending parameter b is statistically compatible with a single value over all phase intervals as found by Massaro et al. (2001)
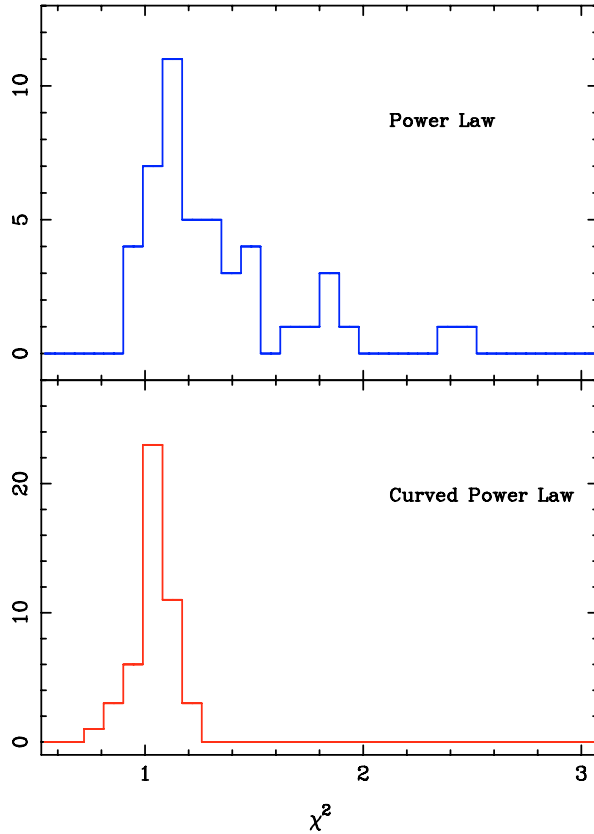
Fig. 4. Frequency histogram of the reduced χ^2 for 256 d.o.f. obtained fitting simultaneously JEM-X2 and IBIS/ISGRI spectra with a single power law (*top panel*) and with the curved model of Eq. (1).

Fig. 5. Best fit parameters a and b measured fitting simultaneously JEM-X2 and IBIS/ISGRI with the curved model of Eq. (1) vs. phase.

over 3 wider intervals. The fit with a constant gave a value of 0.14 ± 0.02, where the error represents the spread around the average.

5. Discussion

INTEGRAL observations of the Crab pulsar provided a high-statistical data set for the study of the spectral and phase distribution of the pulsed emission over a wide X-ray energy interval (3–500 keV). The main result from the analysis of these data is that the pulsed spectral distribution can be accurately represented by a curved function. The values of the bending parameter b in different phase intervals are consistent within the errors with a constant. This is a first independent confirmation of BeppoSAX results presented in Massaro et al. (2000). Other results of the timing and spectral analysis can be summarized in the following points:

- the spectral distribution changes with phase: the photon index softens towards P1, hardens in the Ip region and increases again in the second peak with a characteristic reverse S shape over the 3–500 keV energy range;
- the photon index at the P1 leading edge shows a significative increase both in the JEM-X2 and in the IBIS/ISGRI energy ranges confirming the results obtained by Pravdo et al. (1997) and Massaro et al. (2000) yet questioned by Vivekanand (2002);
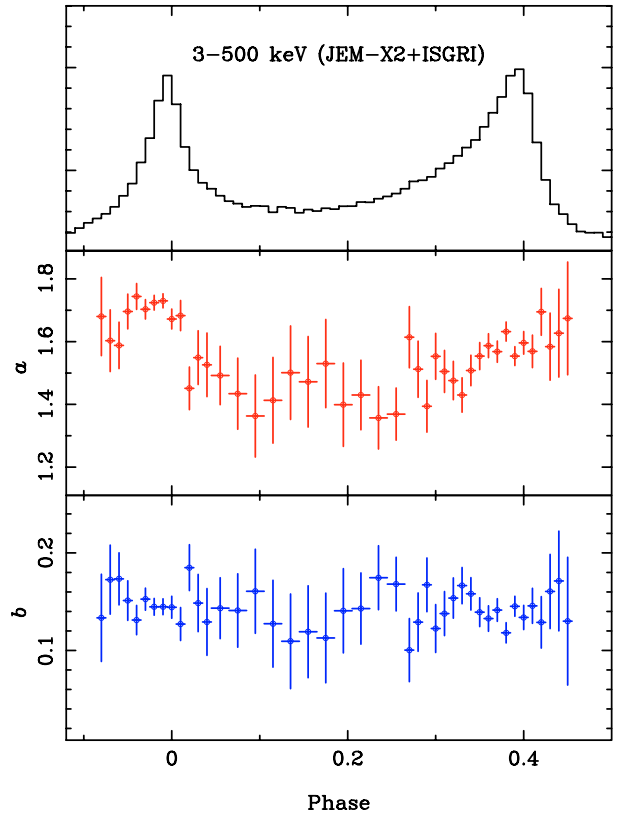
- the analysis of IBIS/ISGRI spectrum relative to the phase interval (0.27–0.47) does not rule out the presence of the 440 keV line detected by Massaro et al. (1991).

The value of the bending parameter (0.14 ± 0.02) is similar to the values obtained for other Crab-like pulsars (de Plaa et al. 2003; Cusumano et al. 2001; Mineo et al. 2004) strongly suggesting a common characteristic of these sources.

A log-parabolic spectrum, can be interpreted in term of the physics of the particle acceleration. It can be obtained when the acceleration decreases with the particle energy Massaro et al. (2004a,b). In the case of the pulsar environment, this could result from several crossings of the magnetosphere gaps with a time of permanence inside the acceleration region that decrease with the energy of the particles.

The Spectral Energy Distribution (SED) of the log-parabolic law has a maximum at the energy E_p given by

$$E_p = 10^{(2-a)/2b}. \tag{2}$$

Considering the variation with phase of the parameter a, the values of E_p ranges between ~10 keV and ~130 keV, in first peak and in the interpeak phase intervals, respectively. A possible explanation of the phase variation of the maximum energy is that we are observing photons emitted at different levels of the magnetosphere. The three-dimensional outer gap model (Cheng et al. 2000) seems to provide a viable theoretical description. In the framework of this model, curvature gamma-rays are converted into electron-positron pairs by the interaction with the magnetic field and X-ray photons are then

radiated by these secondary particles as synchrotron emission with a typical photon energy $E_{\rm syn}$:

$$E_{\rm syn}(r) = \frac{3}{2}\left(\frac{E_{\rm e}}{mc^2}\right)^2 \frac{he\,B(r)\sin\beta(r)}{mc} \tag{3}$$

where $E_{\rm e}$ is the electron energy $B(r)$ is the dipole magnetic field, $\sin\beta(r) \propto (r)^{1/2}$ the pitch angle and r the hight from the star surface within the magnetosphere. Assuming that $E_{\rm e}$ is a fraction of the curvature energy estimated as:

$$E_{\rm cur}(r) = \frac{3}{2}\hbar\gamma_{\rm e}^3(r)\,\frac{c}{s(r)}, \tag{4}$$

where $\gamma_{\rm e}(r) \propto (r)^{-1/8}$ is the local Lorentz factor and $s(r) \propto (r)^{1/2}$ is the curvature radius, the ratio between the two SED maxima can be related to the ratio of the height of the emission regions r_1 and r_2:

$$\frac{E_{\rm syn}(r_1)}{E_{\rm syn}(r_2)} = \frac{E_{\rm cur}(r_1)}{E_{\rm cur}(r_2)}\frac{B(r_1)}{B(r_2)}\frac{\sin\beta(r_1)}{\sin\beta(r_2)}. \tag{5}$$

Introducing the dependence from r of each variable we find the following simplified relation:

$$\frac{E_{\rm syn}(r_1)}{E_{\rm syn}(r_2)} \simeq \left(\frac{r_2}{r_1}\right)^{2.7}. \tag{6}$$

Results from INTEGRAL spectral phase resolved analysis on the two average energies imply a ratio of the heights of emitting regions of ~0.3–0.4 in agreement with the plot in Fig. 9 of Cheng et al. (2000) where the level of the emission region vs. phase computed for the Crab pulsar is shown.

The present analysis of the Crab X-ray pulsed emission confirms that a wide energy band analysis is very important for the study and understanding of the SED of radio pulsars. Future mission sensitive to the γ rays should include this source as a primary scientific target.

References

Brandt, S., Budtz-Jørgensen, C., Lund, N., et al. 2003, A&A, 411, L433
Cheng, K. S., Ruderman, M., & Zhang, L. 2000, ApJ, 537, 964
Cusumano, G., Mineo, T., Massaro, E., et al. 2001, A&A, 375, 397
D'Amico, F., Heindl, W. A., Rothschild, R. E., & Gruber, D. E. 2001, ApJ, 547, L147
de Plaa, J., Kuiper, L., & Hermsen, W. 2003, A&A, 400, 1013
Di Cocco, G., Caroli, E., Celesti, E., et al. 2003, A&A, 411, L189
Dove, J. B., Wilms, J., Nowak, M. A., Vaughan, B. A., & Begelman, M. C. 1998, MNRAS, 298, 729
Galloway, D. K. 2000, ApJ, 543, L137
Goldwurm, A., David, P., Foschini, L., et al. 2003, A&A, 411, L223
Gros, A., Goldwurm, A., Cadolle-Bel, M., et al. 2003, A&A, 411, L179
Kuiper, L., Hermsen, W., Cusumano, G., et al. 2001, A&A, 378, 918
Kuiper, L., Hermsen, W., Walter, R., & Foschini, L. 2003, A&A, 411, L31
Lebrun, F., Leray, J. P., Lavocat, P., et al. 2003, A&A, 411, L141
Lund, N., Budtz-Jørgensen, C., Westergaard, N. J., et al. 2003, A&A, 411, L231
Massaro, E., & Cusumano, G. 2003, in Pulsars, AXPs and SGRs Observed with BeppoSAX and Other Observatories, 15
Massaro, E., Cusumano, G., Litterio, M., & Mineo, T. 2000, A&A, 361, 695
Massaro, E., Litterio, M., Cusumano, G., & Mineo, T. 2001, in Exploring the Gamma-Ray Universe, ESA SP-459, 229
Massaro, E., Matt, G., Salvati, M., et al. 1991, ApJ, 376, L11
Massaro, E., Perri, M., Giommi, P., & Nesci, R. 2004a, A&A, 413, 489
Massaro, E., Perri, M., Giommi, P., Nesci, R., & Verrecchia, F. 2004b, A&A, 422, 103
Mineo, T., Cusumano, G., & Massaro, E. 2004, Nucl. Phys. B Proc. Suppl., 132, 632
Mineo, T., Cusumano, G., Segreto, A., et al. 1997, A&A, 327, L21
Pravdo, S. H., Angelini, L., & Harding, A. K. 1997, ApJ, 491, 808
Rots, A. H., Jahoda, K., & Lyne, A. G. 2004, ApJ, 605, L129
Skinner, G., & Connell, P. 2003, A&A, 411, L123
Strong, A. W. 2003, A&A, 411, L127
Tennant, A. F., Becker, W., Juda, M., et al. 2001, ApJ, 554, L173
Toor, A., & Seward, F. D. 1974, AJ, 79, 995
Ubertini, P., Lebrun, F., Di Cocco, G., et al. 2003, A&A, 411, L131
Ulmer, M. P., Lomatch, S., Matz, S. M., et al. 1994, ApJ, 432, 228
Vedrenne, G., Roques, J.-P., Schönfelder, V., et al. 2003, A&A, 411, L63
Vivekanand, M. 2002, A&A, 391, 1033
Walter, R., Favre, P., Dubath, P., et al. 2003, A&A, 411, L25
Weisskopf, M. C., O'Dell, S. L., Paerels, F., et al. 2004, ApJ, 601, 1050
Westergaard, N. J., Kretschmar, P., Oxborrow, C. A., et al. 2003, A&A, 411, L257
Winkler, C., Courvoisier, T. J.-L., Di Cocco, G., et al. 2003, A&A, 411, L1
Zhang, L., & Cheng, K. S. 2002, ApJ, 569, 872

Online Material

Appendix A: ISGRI energy correction and response matrix

The ISGRI detection layer, that consists of an 128×128 array of independent CdTe detector pixels, suffer of a rather severe "Charge Loss Effect", common to this kind of detectors. To take into account these effects, the solution adopted by the calibration team (Lebrun et al. 2003) is to perform an energy correction as a function of the pulse rise-time using multiplicative coefficients stored in a "Look-Up" Table (LUT2). The version of the LUT2 distributed with the OSA software is not yet optimized[3], and it introduces artificial features in the spectra, the most relevant in the 80 keV region, that are compensated with an ad hoc modifications of the ISGRI effective area[4] (see left panel of Fig. A.1). However, the intensity of the artificial features strongly depend on the spectral shape and the analysis of sources with spectral shapes different from that of the Crab might be affected.

A new LUT2[5] based on on-ground and in-flight calibration data has been generated by one of the authors A. Segreto. The better energy correction is confirmed by the fact that it is no more necessary to introduce ad-hoc wiggles in the effective area, as shown in the right panel of Fig. A.1. Moreover, the new effective area gives a value of the Crab spectral index in better agreement with the one quoted in literature and measured by the other instrument on-board INTEGRAL[6] (see also Table A.1). In Fig. A.2, the residuals of the power law fit of the Crab spectrum obtained processing the ISGRI data with the standard OSA 4.2 response matrix (left panel) and with the A.S. LUT2 and effective area (right panel) are shown.

Tests on this matrix have been performed analysing sources which are detected with good statistics up to 100–200 keV. The spectral parameter derived with the two matrices are plotted in Table A.1 together with the values quoted in literature. The matrix we adopted gives best fit values of the spectral parameters in agreement with the ones quoted in literature and χ^2 values generally lower than the one derived from the standard OSA 4.2 matrix.

---

[3] See A. Segreto talk at the Internal INTEGRAL workshop available at
`http://www.rssd.esa.int/Integral/workshops/Jan2005/`
[4] See the report osa_sci_val_isgri-1.0.pdf available at
`http://isdc.unige.ch/Soft/download/osa/osa_doc/prod`
[5] The file is available from the web page
`http://www.ifc.inaf.it/~ferrigno/integral/`
`ISGRI_alternative_IC`
[6] See the report osa_cross_cal-1.0.pdf available at
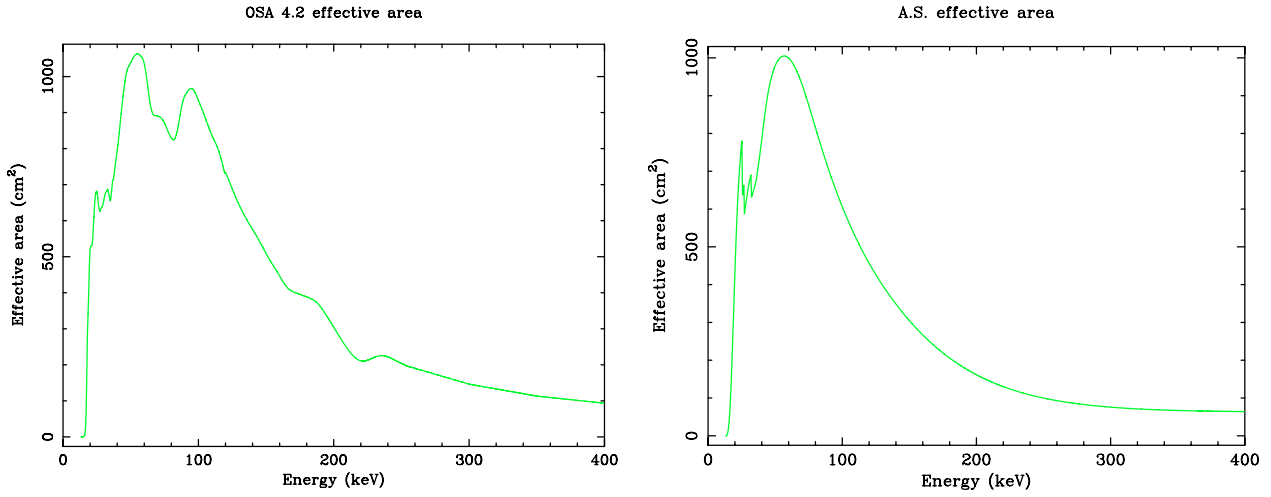`http://isdc.unige.ch/Soft/download/osa/osa_doc/prod/`

Fig. A.1. ISGRI effective area vs. energy for the standard software (*left panel*) and for the A.S. version (*right panel*). Features in the range 30–40 keV are due to CdTe absorption edges.
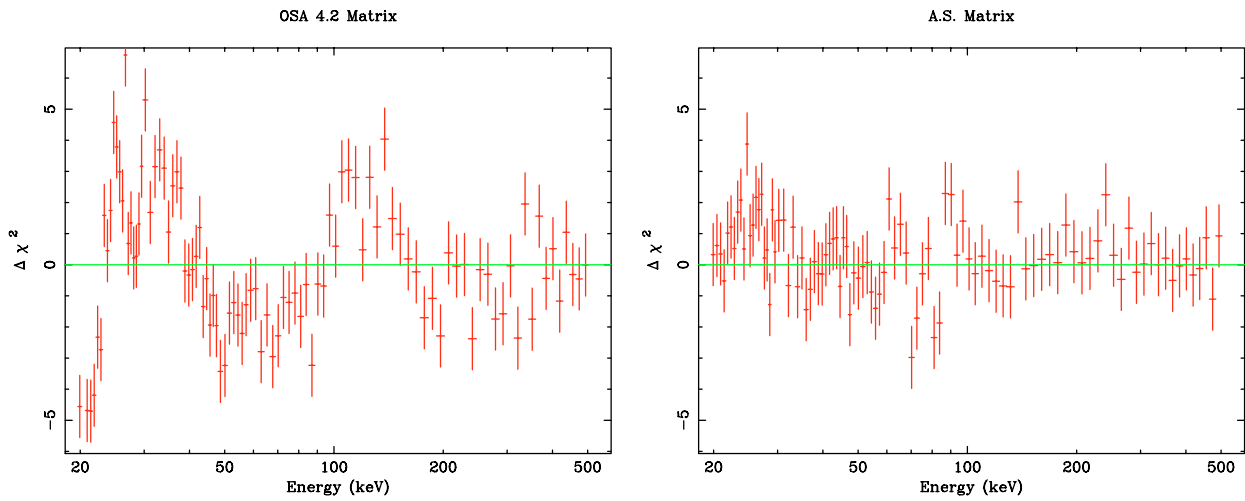

Fig. A.2. *Left panel*: residuals of the power law fit of the Crab spectrum obtained processing ISGRI data with the standard LUT2 and effective area. *Right panel*: residuals of the power law fit of the Crab spectrum obtained processing ISGRI data with the A.S. LUT2 and effective area.

Table A.1. Comparison of the best fit parameters obtained using the standard matrix (ISDC) and the new A.S. version.

Parameter	OSA 4.2	A.S. Version	Other experiment
Crab nebula+pulsar: Power Law			
α	$2.19 \pm 0.03^*$	2.09 ± 0.03	2.1
K (ph cm^{-2} s^{-1} KeV^{-1})	$10.2 \pm 0.2^*$	9.6 ± 0.2	9.7
χ^2 (d.o.f.)	5.6 (95)	1.3 (95)	
			Ref. (1)
GX 1+4: Comptonization continuum model (COMPTT in XSPEC)			
T_0 (keV)	1.27 (frozen)	1.27 (frozen)	$1.27^{+1.4}_{-1.1}$
T_e(keV)	13.5 ± 0.5	12.6 ± 0.4	10.3^{+13}_{-9}
τ	2.7 ± 0.1	3.3 ± 0.2	3.7^{+4}_{-3}
K (ph cm^{-2} s^{-1} KeV^{-1})	$(2.1 \pm 0.1) \times 10^{-2}$	$(1.9 \pm 0.1) \times 10^{-2}$	$2.1^{+2.3}_{-1.8} \times 10^{-2}$
χ^2 (d.o.f.)	1.5 (58)	1.1 (58)	
			Ref. (2)
Cygnus X1: Cut-off power law			
α	$1.66 \pm 0.04^*$	1.45 ± 0.04	1.45 ± 0.01
E_c (keV)	$158 \pm 12^*$	122 ± 7	162 ± 9
K (ph cm^{-2} s^{-1} KeV^{-1})	$1.7 \pm 0.3^*$	1.2 ± 0.3	0.91 ± 0.04
χ^2 (d.o.f.)	3.2 (48)	1.9 (48)	
			Ref. (3)
Sco X1: Bremstralung + Power law			
KT (keV)	4.2 ± 0.1	4.3 ± 0.1	4.51 ± 0.08
Flux$_{20-50 \text{ keV}}$ (erg cm^{-2} s^{-1})	$(5.5 \pm 0.3) \times 10^{-9}$	$(6.5 \pm 0.4) \times 10^{-9}$	$(7.4 \pm 0.6) \times 10^{-9}$
α	2.9 ± 0.2	2.8 ± 0.2	2.4 ± 0.3
Flux$_{20-200 \text{ keV}}$ [erg cm^{-2} s^{-1}]	$(0.8 \pm 0.4) \times 10^{-9}$	$(0.7 \pm 0.4) \times 10^{-9}$	$(1.04 \pm 0.08) \times 10^{-9}$
χ^2 (d.o.f.)	1.3 (52)	1.4 (52)	
			Ref. (4)

* Errors are computed introducing systematic errors in order to reduce the χ^2 below 2.0.
(1) Toor & Seward (1974); (2) Galloway (2000); (3) Dove et al. (1998); (4) D'Amico et al. (2001).